LIMNOLOGY AND OCEANOGRAPHY
Letters

ASLO
Open Access

Limnology and Oceanography Letters 3, 2018, 31–38

doi: 10.1002/lol2.10067

LETTER

Response of a fringing reef coastline to the direct impact of a tropical cyclone

M. V. W. Cuttler [1,2]* *J. E. Hansen* [1] *R. J. Lowe,* [1,2] *E. J. F. Drost* [1,2]

[1]UWA Oceans Institute and School of Earth Sciences, The University of Western Australia, Crawley, Western Australia, Australia; [2]ARC Centre of Excellence for Coral Reef Studies, The University of Western Australia, Crawley, Western Australia, Australia

Scientific Significance Statement

Tropical cyclones can have catastrophic consequences for coastal infrastructure, marine habitats, and coastal populations worldwide. However, coral reefs can provide natural coastal protection by reducing the amount of wave energy reaching coastlines. Here, we quantify the coastal protection afforded by a fringing reef from a direct tropical cyclone impact and show that the observed beach erosion was not associated with the magnitude of the extreme offshore waves, but rather due to local wind wave growth across the lagoon. These results can be applied to assess coastal hazards facing reef-fringed coastlines due to extreme tropical cyclone conditions and will become increasingly relevant as climate change alters the status of coral reefs globally.

Abstract

Tropical cyclones generate extreme hazards along coastlines, often leading to losses of life and property. Although coral reefs exist in cyclone-prone regions globally, few studies have measured the hydrodynamic conditions and morphological responses of reef-fringed coastlines to tropical cyclones. Here, we examine the impact of Tropical Cyclone Olwyn on a section of Australia's largest fringing reef (Ningaloo Reef) using in situ wave and water level observations, topographic surveys, and numerical modeling. Despite forereef significant wave heights reaching 6 m and local winds of 140 km h^{-1}, average beach volume change was only -3 m^3 m^{-1}. The results indicate that this erosion was due to locally generated wind waves within the lagoon rather than the offshore waves that were dissipated on the reef crest. A comparison of these volume changes to observations of tropical cyclone impacts along exposed sandy beaches quantitatively demonstrates the substantial coastal protection reefs can provide against extreme storms.

The coastal impacts of tropical cyclones (TCs), namely erosion, flooding, and habitat destruction, have been well documented globally (Castillo et al. 2012; Woodruff et al. 2013). Existing studies of TC impacts on coral reef-fringed coastlines have primarily focused on the impact to the coral communities (Harmelin-Vivien 1994), the hydrodynamic

*Correspondence: michael.cuttler@uwa.edu.au

Author Contribution Statement: MVWC collected and analyzed the field data, developed and analyzed the numerical model, and wrote the manuscript. JEH helped with data analysis and interpretation, model development and analysis, and provided critical review of the manuscript. RJL helped with experimental design, data and model interpretation, and provided critical review of the manuscript. EJFD developed the regional-scale model and helped with development and validation of the local model.

Data Availability Statement: The metadata and specific data files used in the analyses described in the text and Supporting Information are accessible at https://doi.org/10.5281/zenodo.1162945

Additional Supporting Information may be found in the online version of this article.

conditions over the reefs (Péquignet et al. 2011), or the fate of storm deposits (Scoffin 1993). However, few studies have focused on the hydrodynamic and morphodynamic processes driving changes in reef-fringed beach morphology during a TC. In this study, we quantify the morphological change due to a direct cyclone impact along a reef-fringed coast, identify the physical mechanisms responsible for the observed beach erosion patterns, and assess the coastal protection provided by the reef relative to exposed sandy coasts experiencing similar extreme met-ocean conditions.

Fringing reefs, which can range from shore-attached to several kilometers offshore, are the most prevalent class of coral reefs along tropical coasts (Hopley 2004). Reefs provide natural coastal protection by dissipating offshore wave energy through both wave breaking and bottom friction (Lowe et al. 2005; Rogers et al. 2016). Despite the abundance of reef hydrodynamic studies, few studies have quantified the processes governing coastal morphological changes in reefs, particularly during TCs. Previous studies conducted under more typical (non-TC) conditions have shown that shorelines fringed by reefs can experience morphological changes on short (weekly) to intermediate (seasonal) timescales due to changes in wind and wave direction (Eversole and Fletcher 2003; Beetham and Kench 2014); and that reef-fronted beaches are generally more stable than exposed beaches (Ruiz de Alegria-Arzaburu et al. 2013). The limited studies that have directly measured TC-induced shoreline changes have suggested that shoreline response is inversely related to reef flat width, with the magnitude of beach erosion decreasing with increasing reef flat width (Mahabot et al. 2016). These same studies have also suggested that the relative coastline orientation (i.e., in relation to local wind and wave direction) can influence the magnitude of coastal erosion. However, due to the episodic nature of TCs and the rarity of capturing a direct impact with in situ instrumentation, there still remains a gap in understanding of how much coastal protection is offered by fringing reefs during TCs, and moreover, which factors specifically govern coastal responses.

Rigorously assessing the coastal protection afforded by reefs is particularly important given that a number of recent studies have suggested that the coastal protection offered by reefs is under threat due to both coral degradation (i.e., declining rates of net reef accretion and decreasing bottom roughness) and sea level rise, which will increase submergence depths and therefore expose reef-protected coastlines to larger waves (Grady et al. 2013; Quataert et al. 2015). Collectively, these studies emphasize that it is critical to understand the physical drivers of morphologic change in reef environments to better predict future changes to these coastlines. In this study, we combine in situ measurements (wave heights, water levels), repetitive topographic beach surveys, and numerical simulations from a coupled wave-current model (Delft3D/SWAN) to quantify the coastal response from the direct impact of TC Olwyn (2015) at Ningaloo Reef, Western Australia.

Data and methods

Study area

Ningaloo Reef is Australia's largest fringing reef, stretching $\sim$ 270 km south from Australia's North West Cape (Fig. 1a). The morphology of Ningaloo is characterized by a steep (1 : 20) forereef slope, a relatively narrow reef flat (100s of m), and a wide (1–5 km), but shallow ($<$ 5 m deep) lagoon (Collins et al. 2003). The study area is located at the northern end of Ningaloo Reef at Tantabiddi (Fig. 1c) and features a shoreline salient inland from the reef flat; a common feature along the reef-fringed coastline of Western Australia, including at Ningaloo (Sanderson 2000). The beach has a variable slope (calculated between the 0.5 m and 1.5 m contours), ranging from $\sim$ 0.03 north of the salient to $\sim$ 0.15 south of the salient, is relatively narrow ($\leq$ 100 m), and is backed by a dune system (heights from 3 m to 10 m). Ningaloo Reef experiences small tides (average range $\sim$ 0.8 m) with typical incident waves heights of 1–2 m from a southwesterly direction; however, waves often reach $\sim$ 4 m during austral winter swell events (Taebi et al. 2012). Depth-induced breaking on the shallow reef crest drives onshore flow across the reef flat toward the lagoon; within the lagoon, currents typically diverge at the salient toward the adjacent channels (Taebi et al. 2011). The sediment at Tantabiddi is dominated by biogenic material (70–95%), with an average density of 2.58 g cm^{-3} (Cuttler et al. 2017). The spatial distribution of sediment at Tantabiddi generally follows the mean current patterns, with the coarsest material (median grain size, D_{50}, $\sim$ 0.5 mm) found on the outer reef flat, and finer material found within the lagoon (D_{50} $\sim$ 0.35 mm) and on the beach (D_{50} $\sim$ 0.23 mm) (Cuttler et al. 2017).

Ningaloo Reef is located along Australia's Northwest Shelf, which is the most cyclone prone region of Australia, experiencing 1–2 TCs per year (Drost et al. 2017). In order to opportunistically capture the impact of a TC on this reef-fronted coastline, five pressure sensors (Fig. 1c,d) were deployed from December 2014 to May 2015. On 11 March 2015, TC Olwyn developed off the northwest coast and tracked southward until crossing land on 13 March 2015 (Fig. 1a,b). On 12 March 2015, its eye passed $\sim$ 10 km to the west (offshore) of the study area (Fig. 1b) as a Category 3 (Australian tropical cyclone intensity scale) cyclone with an estimated central pressure of 965 hpa, sustained winds of 140 km h^{-1}, and gusts up to 200 km h^{-1}.

Meteorological and hydrodynamic data

Meteorological data (atmospheric pressure, wind speed, and wind direction) were measured $\sim$ 18 km south of the study site at the Milyering weather station, maintained by the Australian Institute of Marine Science. A cross-shore

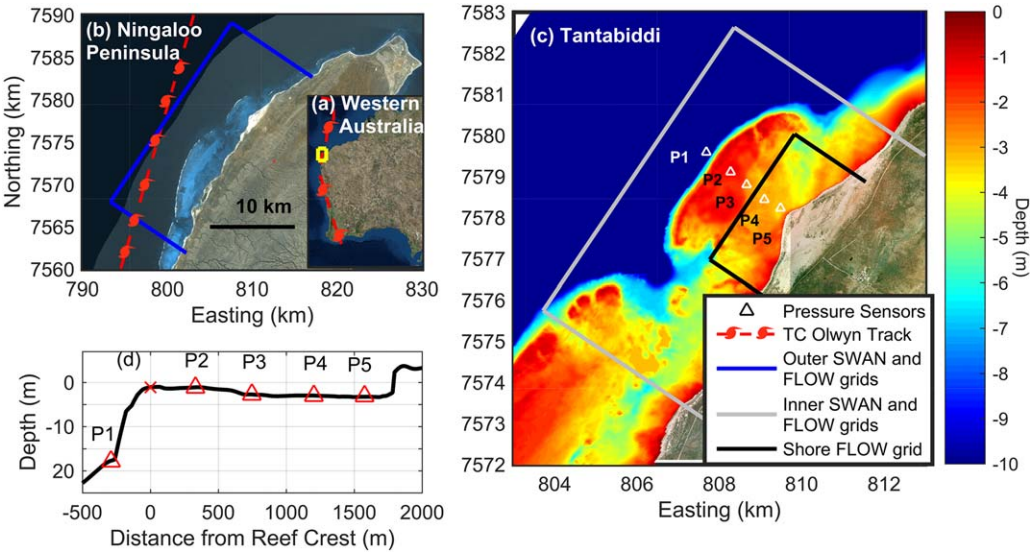

Fig. 1. (**a**) Western Australia with the Ningaloo Peninsula in yellow; (**b**) the Ningaloo Peninsula with the boundaries of the "outer" Delft3D-FLOW and SWAN domain indicated in blue; (**c**) study site and bathymetry with the cross-shore array of pressure sensors indicated by the white triangles, the "inner" Delft3D-FLOW and SWAN domain show in gray and the "shore" Delft3D-FLOW grid shown in black. TC Olwyn track is the red line in (**a**) and (**b**). (**d**) Cross-shore depth profile from the coastline to the forereef, with the reef crest marked with a red "x" and pressure sensors denoted by red triangles.

array of pressure sensors (RBR*virtuoso*), extending from the forereef (~ 18 m depth) to the shoreline recorded observations of waves and water levels (Fig. 1c,d). All sensors logged continuously at 1 Hz until 19 March 2015 when they were recovered following TC Olwyn. Atmospheric pressure was removed from the pressure observations and the tidal component of the water level was removed using the time series predicted by T_TIDE (Pawlowicz et al. 2002) with constituents derived from the forereef pressure sensor. Hourly estimates of the sea surface energy-frequency spectrum were obtained from Fourier transforms of 1-h de-meaned and detided data segments and block averaged using a Hamming window (1024 samples) with 50% overlap, yielding 17 degrees of freedom (Thomson and Emery 2014). Hourly significant wave heights were estimated from the variance of sea surface elevation in the sea-swell (SS; 0.04 Hz $< f <$ 0.4 Hz, where f is frequency) and infragravity (IG; 0.002 Hz $< f <$ 0.04 Hz) energy bands ($H_{sig,SS}$ and $H_{sig,IG}$, respectively) using linear wave theory.

The pressure observations were also used to estimate setup following:

$$\overline{\eta} = \overline{h_{tot}} - \overline{\eta}_t - h_o \quad (1)$$

where $\overline{\eta}$ denotes setup (due to both waves and wind), $\overline{h_{tot}}$ is total measured depth (assuming hydrostatic pressure), $\overline{\eta_t}$ denotes tidal elevation, h_o is still water level, and overbars denote hourly averaging. Still water level (h_o) is a constant at each site and was calculated as the depth at each site when forereef waves were low ($H_{sig,SS} < 0.8$ m), wind speed was low (< 10 km h^{-1}), and tidal elevation was highest ($\overline{\eta_t} > 0.6$ m; i.e., assuming no wave setup) (Raubenheimer et al. 2001). All measurements were then referenced to the forereef sensor to remove any water level fluctuations due to shelf-scale water level variations (Lowe et al. 2009).

Beach morphologic changes

Annual beach surveys have been conducted at Tantabiddi since August 2013 using a backpack-mounted differential GPS (DGPS) receiver. The pre-cyclone morphology was recorded in July 2014, approximately 8 months prior to the cyclone, and a "post-cyclone" survey was conducted 10 d after TC Olwyn. Two subsequent "cyclone recovery" surveys were conducted in October 2015 and June 2016. Although the pre-cyclone survey was conducted 8 months prior to TC Olwyn, there were no significant storms (i.e., TCs) in this period, typical large winter swell events (H_{sig} ~ 4–5 m) have minimal erosion potential ("Model simulations" section), and analysis of historical aerial imagery (from 1969 to 2014) of the Tantabiddi salient using the "Digital Shoreline Analysis System" (Thieler et al. 2009) as well as previous work along the greater Ningaloo coastline (Sanderson 2000) provides no evidence to suggest significant seasonal variability in shoreline position (Supporting Information Fig. S1).

Positions from the DGPS surveys (uncertainty of 0.05 m in the vertical and horizontal directions) were organized into a triangulated irregular network and gridded to produce a 1 m cell-size topographic surface of the surveyed beach. Successive topographic surfaces were differenced to determine

the location and extent of erosion or accretion. For the entire ~ 3.5 km beach length studied, 69 cross-shore transects were extracted at 50 m alongshore intervals from the survey grids to assess beach elevation and volume change. Height data were referenced to the Australian height datum (approximately mean sea level).

Numerical model

The numerical model Delft3D-FLOW (Lesser et al. 2004) coupled with the wave model SWAN (Booij et al. 1999) was used to simulate the hydrodynamic conditions during the cyclone. Delft3D solves the unsteady shallow-water equations in two- or three-dimensions (Lesser et al. 2004) and has been used effectively in coral reef environments under both non-storm and storm conditions (Grady et al. 2013; Hoeke et al. 2015). Numerical details, governing equations, and underlying assumptions of Delft3D are described in detail in Lesser et al. (2004); brief details of the model resolution and settings used for this study are described below. Further details of model settings and validation are provided in the Supporting Information.

Delft3D-FLOW (version 6.02.02.5562M) was run in depth-averaged mode and consisted of three domains ("outer," "inner," "shore") of varying resolution that were two-way coupled using "domain decomposition" (Hummel and de Goede 2000). The "outer" domain had a 50 × 50 m resolution, the "inner" domain had a 17 × 17 m resolution, and the "shore" domain had a 5 × 5 m resolution (Fig. 1b,c). The hydrodynamic model was two-way coupled with SWAN (version 40.72) over two nested domains that had the same resolutions as the "outer" and "inner" circulation domains. Stationary SWAN simulations were run at 60 min intervals using updated currents, water levels, and wind from Delft3D-FLOW; wave simulation results were then passed back to Delft3D-FLOW. Although SWAN does not model IG energy, which has been shown to be important to lagoonal processes under non-TC conditions (Pomeroy et al. 2012), it does account for wind-wave growth, which we show below to be a more critical factor in determining the coastal response from TC Olwyn. Model performance was evaluated using the Murphy (1988) Skill Score (Supporting Information Text S2). Inclusion of wind growth yielded the most accurate model results (Supporting Information Table S1, Supporting Information Fig. S2); therefore, all model results presented below (unless otherwise stated) are for simulations with wind growth.

Results

Field observations

The eye of TC Olwyn passed ~ 10 km offshore of the study site on 12 March 2015 (Fig. 1b) and resulted in incident waves on the forereef reaching 5.8 m ($H_{sig,SS}$). To place the TC Olwyn conditions in the context of typical wave conditions ($H_{sig,SS}$ ~ 1–2 m, Pomeroy et al. 2012), the observed

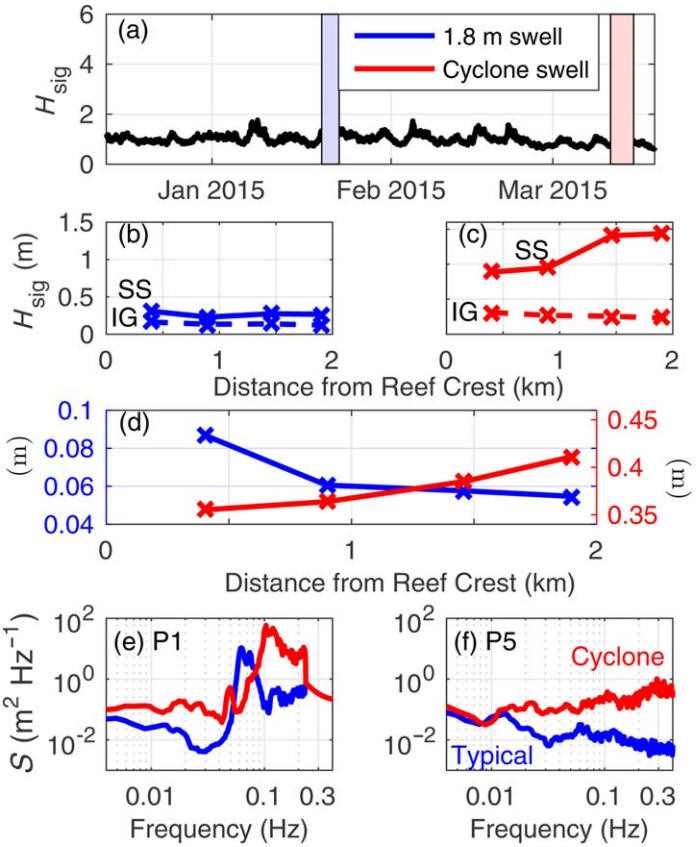

Fig. 2. (**a**) H_{sig} at the forereef pressure sensor (18 m depth) from December 2014 to March 2015, with a typical swell event ($H_{sig,SS}$ ~ 1.8 m) denoted by the blue shading and TC Olwyn ($H_{sig,SS}$ = 5.8 m) denoted by the red shading. (**b**) Cross-shore profiles of $H_{sig,SS}$ (solid line) and $H_{sig,IG}$ (dashed line) within the lagoon (instrument locations indicated by "x") during the (**b**) typical and (**c**) cyclone events. (**d**) Cross-shore profiles of setup during a typical (blue) and cyclone (red) swell event (note different scales). Wave spectra for the (**e**) forereef and (**f**) the shoreline sensors from the 1 h interval when waves were largest during the typical (blue) and cyclone (red) events.

waves and water levels during the cyclone were compared to a "typical" swell event ($H_{sig,SS}$ = 1.8 m) that occurred prior to TC Olwyn (Fig. 2). The cross-shore distribution of wave heights and setup (due to both wind and waves) were considerably different during the TC compared to typical swell conditions. Under typical swell conditions, after dissipation of incident wave energy commences near the reef crest, $H_{sig,SS}$ continues to decrease across the reef flat and lagoon toward shore with $H_{sig,SS}$ and $H_{sig,IG}$ becoming comparable in magnitude (Fig. 2b). However, at the peak of TC Olwyn, although $H_{sig,SS}$ decreased near the reef crest by 89% due to depth-induced wave breaking, $H_{sig,SS}$ increased across the lagoon toward the shoreline, with $H_{sig,SS}$ reaching 1.5 m (~ 1.5 times reef flat $H_{sig,SS}$), or approximately six times larger than $H_{sig,IG}$ (Fig. 2c).

The shoreward growth in $H_{sig,SS}$ corresponded to a change in the wind direction that increased the shoreward-directed

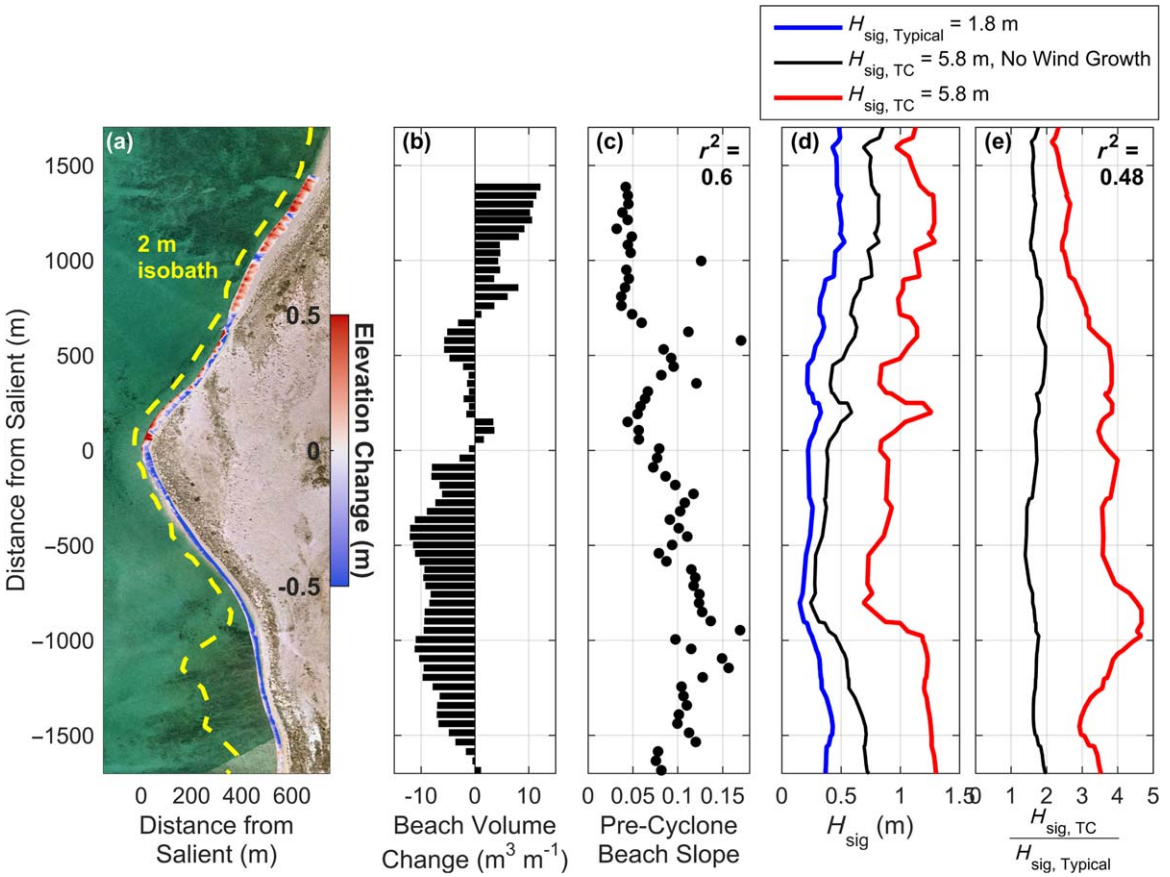

Fig. 3. (**a**) Observed beach elevation change (colors). (**b**) TC-induced beach volume change from July 2014 to March 2015 and (**c**) pre-storm beach slope (β), calculated between the 1.5 m and the 0.5 m contours [the r^2 is between the β and beach volume change shown in (**b**)]. (**d**) Model-predicted H_{sig} along the 2 m isobath [yellow dashed line in (**a**)] for a 1.8 m swell (blue line) and peak TC conditions with (red line) and without wind growth (black line). (**e**) Disequilibrium wave heights ($H_{sig,TC}/H_{sig,Typical}$) predicted with (red line) and without (black line) wind growth [i.e., ratio of red or black line in (**d**) to blue line in (**d**)]; the r^2 is calculated between the disequilibrium TC wave heights with wind growth (red line) and post-cyclone beach volume change [data shown in (**b**)].

component of the wind vector (Supporting Information Fig. S3d). The observed wave spectra show that energy was primarily enhanced at high frequencies (0.1–0.3 Hz) indicating local growth of wind waves within the lagoon (Fig. 2f). Maximum TC waves occurred during high tide (Supporting Information Fig. S3b), which would have allowed more wave energy to propagate into the lagoon and aided wind growth by increasing the lagoon depth. A similar pattern was observed in the cross-shore setup profile. Under typical conditions setup decreased across the lagoon toward the shoreline whereas during the cyclone setup increased toward shore, coincident with the shoreward increasing wave heights and onshore winds (Fig. 2d).

The observed changes in beach morphology were remarkably modest in response to the TC, with alongshore-averaged, sub-aerial profile volume changes of only -3 m^3 m^{-1} and net volume change (integrated over the entire sub-aerial beach) of $-14{,}457$ m^3 (-8%); however, the beach response was variable alongshore (Fig. 3a,b). The north side of the salient showed slight accretion ($+3$ m^3 m^{-1} on average), whereas the south side was predominantly eroded (-8 m^3 m^{-1}; Fig. 3a,b). In regions where erosion occurred, it corresponded to a flattening of the cross-shore beach profile, primarily due to erosion of the dune (removing up to 1.5 m elevation; Supporting Information Fig. S4).

The second post-cyclone survey (October 2015) showed limited beach recovery, with a total sub-aerial beach volume change of $+3885$ m^3 ($+2\%$) from to March 2015; which is still -6% compared to the pre-cyclone beach volume. However, the limited recovery was likely impacted by TC Quang, which passed by the study area $\sim$ 6 weeks after TC Olwyn and had a similar magnitude and storm track. Although the October 2015 profiles showed alongshore-averaged, net erosion compared to July 2014 (-2 m^3 m^{-1}), profiles between 0 m and -600 m (i.e., locations of largest cyclone-induced erosion, Fig. 3b) actually returned to pre-cyclone volumes ($+11$ m^3 m^{-1} recovery from March 2015; Supporting Information Fig. S4d). The final survey (June 2016) showed

complete beach volume recovery, with a total sub-aerial beach volume change of +26,677 m^3 (15% net accretion) compared to the pre-cyclone (July 2014) beach volume.

Model simulations

To further investigate how the nearshore wave fields likely drove the observed spatial variability in beach changes, we used the numerical model to extend the in situ results over the entire study area. Modeled wave heights were extracted along the 2 m isobaths (as an indicator of the wave energy along the beach), which is farther offshore on the south side of the salient due to the southern portion of the lagoon generally being shallower than the north (Fig. 3a).

Modeled wave heights during TC Olwyn were slightly larger on the northern side of the salient, despite the observations indicating accretion in this area (Fig. 3d; Supporting Information Fig. S5). Examination of the alongshore beach morphology showed that TC-induced beach volume change was significantly correlated with the pre-cyclone beach slope ($r^2 = 0.60$, $p \ll 0.01$); with northern (accreted) beaches having shallower slopes and the southern (eroded) beaches having steeper slopes (Fig. 3b,c). Under typical wave conditions, the shoreline on the southern side of the salient ($y = -1000$ m to 0 m) is exposed to smaller waves than the northern side ($y > 0$ m; Fig. 3d), likely explaining the typical alongshore variability in beach slope (Wright and Short 1984). Note, there are no significant alongshore differences in beach sediment characteristics (Cuttler et al. 2017). The largest waves within the lagoon, and likely the majority of the beach morphology changes, occurred when the onshore component of the wind was strongest (Supporting Information Fig. S3); at this time, the wave direction (along the 2 m isobath) was approximately orthogonal to the shoreline (Supporting Information Fig. S5). These results suggest that this reef-fronted beach is in equilibrium with the prevailing conditions, and that the morphological response to TC Olwyn was determined by how much the cyclone waves locally deviated from typical conditions, i.e., the alongshore beach morphological response was related to the spatial pattern in the disequilibrium of TC wave heights ($H_{sig,TC}/H_{sig,Typical}$) from a typical swell event ($r^2 = 0.48$, $p \ll 0.01$; Fig. 3e).

To confirm the role of wind-wave growth within the lagoon, SWAN was run with and without wind growth. Without wind growth included in the model, the nearshore wave heights from the cyclone swell are predicted to be approximately two times larger than during a typical incident swell and disequilibrium wave heights are similar on both sides of the salient. However, with wind growth enabled, nearshore TC wave heights are up to five times larger than those from a typical swell, and the magnitude of disequilibrium from typical conditions is larger on the southern side of the salient, consistent with the observed beach erosion (Fig. 3e). Thus, despite the lagoon being relatively shallow (< 5 m), locally generated wind waves within the lagoon were a dominant mechanism driving the observed beach changes.

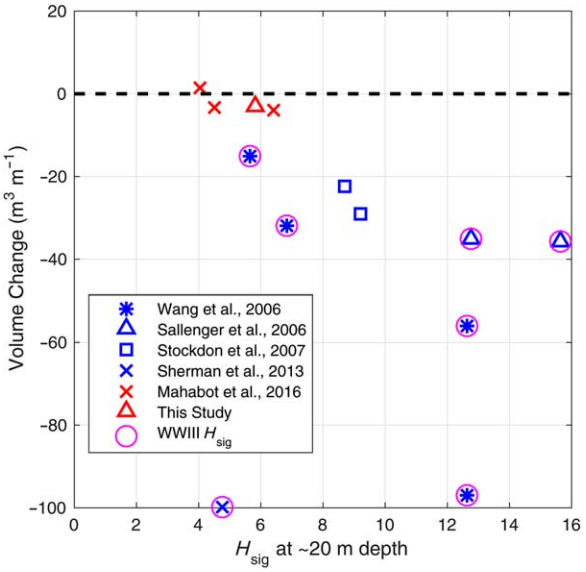

Fig. 4. Comparison of TC-induced beach volume change on open, sandy coasts (blue symbols) and reef-fronted coasts (red symbols). For studies that did not report offshore H_{sig}, wave heights from WaveWatch-III hindcast model predictions (Tolman 2009; ftp://polar.ncep.noaa.gov/pub/history/waves/nww3/) were extracted at the grid cell nearest to the study location in ~ 20 m depth (magenta circles). Values for Mahabot et al. (2016) represent alongshore-averaged values for transects where reef morphology is constant.

Discussion and conclusions

This study highlights the effectiveness of coral reefs at providing natural coastal protection. Despite the extreme offshore wave conditions, beach morphology changes were relatively modest; particularly when compared to the responses of open, sandy coastlines exposed to comparable wave conditions (Fig. 4). For example, average beach volume loss at Tantabiddi was 3 m^3 m^{-1}, whereas, areas in Florida, U.S.A. that were impacted by similar offshore wave heights from Hurricane Ivan experienced ~ 5–10 times greater beach erosion (Wang et al. 2006), with comparable erosion rates also observed during other Atlantic Ocean TCs (blue symbols, Fig. 4). Although the magnitude of beach response in reef environments is much less than sandy environments, the underlying forcing mechanism appears to be similar, with the magnitude of divergence (or disequilibrium) of nearshore wave heights from typical nearshore wave heights a key factor determining storm-induced beach response (e.g., Yates et al. 2009).

The magnitude of beach response observed here agrees well with the few previous observations of TC-induced beach morphology changes in fringing reefs (Fig. 4, red x's) (Mahabot et al. 2016). These previous observations were conducted in shore-attached (i.e., no significant lagoon) reef systems

and highlighted the importance of wave direction and reef flat width in determining morphological response; however here, in a system with a significant lagoon, we suggest that wind-driven processes can also be very significant (or dominant) in driving beach morphodynamics during a TC. We note that the influence of these wind-driven processes will likely scale with distance from the TC and lagoon width. For example, if TC Olwyn had passed further offshore of the study site, incident wave heights may have been similar (i.e., $\sim$ 6 m) but local winds would have been much less. Therefore, nearshore wave heights would have been significantly smaller and beach volume changes likely would have been even less than those observed here.

These results show that the offshore TC-generated waves were largely dissipated by the reef and played a minimal role in driving the beach changes. Instead, locally generated wind waves played a critical role in determining the morphological change, with the wind waves reaching the shoreline ultimately being larger than the residual offshore waves that were transmitted across the reef. Although future climate changes are likely to increase wave transmission over coral reefs, primarily due to sea level rise but also due to degradation of reef habitats (Grady et al. 2013; Quataert et al. 2015), the results presented here show that while these structures still exist, they can provide natural coastal protection from offshore waves, even under extreme conditions. However, our results also reveal that even over the small scales (order 1 km) of a nearshore reef-lagoon system, local wind wave generation can play a dominant role in sediment transport and erosion responses during TC conditions, a process traditionally neglected in nearshore model applications to predict beach response to extreme events (e.g., models that can only consider remotely generated waves, such as Xbeach). Furthermore, because the reef geomorphology at Ningaloo (e.g., shallow reef crest that gradually deepens to a shallow lagoon) represents a "standard" reef (Falter et al. 2013), accounting for the local wind growth of waves is expected to be critical to determining beach response to TCs in reef systems worldwide.

References

Beetham, E. P., and P. S. Kench. 2014. Wave energy gradients and shoreline change on Vabbinfaru platform, Maldives. Geomorphology **209**: 98–110. doi:10.1016/j.geomorph.2013.11.029

Booij, N., R. C. Ris, and L. H. Holthuijsen. 1999. A third-generation wave model for coastal regions: 1. Model description and validation. J. Geophys. Res. Oceans **104**: 7649–7666. doi:10.1029/98JC02622

Castillo, M. E., E. M. Baldwin, R. S. Casarin, G. P. Vanegas, and M. A. Juaréz. 2012. Characterization of risks in coastal zones: A review. Clean Soil Air Water **40**: 894–905. doi:10.1002/clen.201100679

Collins, L. B., Z. R. Zhu, K.-H. Wyrwoll, and A. Eisenhauer. 2003. Late Quaternary structure and development of the northern Ningaloo Reef, Australia. Sediment. Geol. **159**: 81–94. doi:10.1016/S0037-0738(03)00096-4

Cuttler, M. V. W., R. J. Lowe, J. L. Falter, and D. Buscombe. 2017. Estimating the settling velocity of bioclastic sediment using common grain-size analysis techniques. Sedimentology **64**: 987–1004. doi:10.1111/sed.12338

Drost, E. J. F., R. J. Lowe, G. N. Ivey, N. L. Jones, and C. A. Pequignet. 2017. The effects of tropical cyclone characteristics on the surface wave fields in Australia's North West region. Cont. Shelf Res. **139**: 35–53. doi:10.1016/j.csr.2017.03.006

Eversole, D., and C. H. Fletcher. 2003. Longshore sediment transport rates on a reef-fronted beach: Field data and empirical models Kaanapali Beach, Hawaii. J. Coast. Res. **19**: 649–663.

Falter, J. L., R. J. Lowe, Z. Zhang, and M. McCulloch. 2013. Physical and Biological Controls on the Carbonate Chemistry of Coral Reef Waters: Effects of Metabolism, Wave Forcing, Sea Level, and Geomorphology. PLoS ONE **8**: e53303. doi:10.1371/journal.pone.0053303

Grady, A. E., L. J. Moore, C. D. Storlazzi, E. Elias, and M. A. Reidenbach. 2013. The influence of sea level rise and changes in fringing reef morphology on gradients in alongshore sediment transport. Geophys. Res. Lett. **40**: 3096–3101. doi:10.1002/grl.50577

Harmelin-Vivien, M. L. 1994. The effects of storms and cyclones on coral reefs: A Review. J. Coast. Res. 211–231.

Hoeke, R., K. McInnes, and J. O'Grady. 2015. Wind and wave setup contributions to extreme sea levels at a tropical high island: A stochastic cyclone simulation study for Apia, Samoa. J. Mar. Sci. Eng. **3**: 1117–1135. doi:10.3390/jmse3031117

Hopley, D. 2004. Coral reefs, p. 343–349. *In* M. A. Schwarz [ed.], Encyclopedia of coastal science. Springer.

Hummel, S., and E. D. de Goede. 2000. Domain decomposition with grid refinement for shallow water modeling. *In* Proceedings of the 4th International Conference on Hydroinformatics, Iowa City, USA, July 23–27, 2000. Iowa Institute of Hydraulic Research.

Lesser, G. R., J. A. Roelvink, J.A.T.M. van Kester, and G. S. Stelling. 2004. Development and validation of a three-dimensional morphological model. Coast. Eng. **51**: 883–915. doi:10.1016/j.coastaleng.2004.07.014

Lowe, R. J., J. L. Falter, M. D. Bandet, G. Pawlak, M. J. Atkinson, S. G. Monismith, and J. R. Koseff. 2005. Spectral wave dissipation over a barrier reef. J. Geophys. Res. **110**: C04001. doi:10.1029/2004JC002711

Lowe, R. J., J. L. Falter, S. G. Monismith, and M. J. Atkinson. 2009. Wave-driven circulation of a coastal reef – lagoon system. J. Phys. Oceanogr. **39**: 873–893. doi:10.1175/2008JPO3958.1

Mahabot, M.-M., G. Pennober, S. Suanez, R. Troadec, and C. Delacourt. 2016. Effect of tropical cyclones on short-term evolution of carbonate sandy beaches on Reunion Island, Indian Ocean. J. Coast. Res. **33**: 839–853. doi:10.2112/JCOASTRES-D-16-00031.1

Murphy, A. H. 1988. Skill scores based on the mean square error and their relationships to the correlation coefficient. Monthly weather review **116.12**: 2417–2424.

Pawlowicz, R., B. Beardsley, and S. Lentz. 2002. Classical tidal harmonic analysis including error estimates in MATLAB using T_TIDE. Comput. Geosci. **28**: 929–937. doi:10.1016/S0098-3004(02)00013-4

Péquignet, A. C., J. M. Becker, M. A. Merrifield, and S. J. Boc. 2011. The dissipation of wind wave energy across a fringing reef at Ipan, Guam. Coral Reefs **30**: 71–82. doi:10.1007/s00338-011-0719-5

Pomeroy, A., R. Lowe, G. Symonds, A. Van Dongeren, and C. Moore. 2012. The dynamics of infragravity wave transformation over a fringing reef. J. Geophys. Res. **117**: C11022. doi:10.1029/2012JC008310

Quataert, E., C. Storlazzi, A. van Rooijen, O. Cheriton, and A. van Dongeren. 2015. The influence of coral reefs and climate change on wave-driven flooding of tropical coastlines. Geophys. Res. Lett. **42**: 6407–6415. doi:10.1002/2015GL064861

Raubenheimer, B., R. T. Guza, and S. Elgar. 2001. Field observations of wave-driven setdown and setup. J. Geophys. Res. **106**: 4629–4638. doi:10.1029/2000JC000572

Rogers, J. S., S. G. Monismith, D. A. Koweek, and R. B. Dunbar. 2016. Wave dynamics of a Pacific Atoll with high frictional effects. J. Geophys. Res. Oceans **121**: 350–367. doi:10.1002/2015JC011170

Ruiz de Alegria-Arzaburu, A., I. Mariño-Tapia, C. Enriquez, R. Silva, and M. González-Leija. 2013. The role of fringing coral reefs on beach morphodynamics. Geomorphology **198**: 69–83. doi:10.1016/j.geomorph.2013.05.013

Sanderson, P. G. 2000. A comparison of reef-protected environments in Western Australia: The central west and Ningaloo coasts. Earth Surf. Process. Landforms **25**: 397–419. doi:10.1002/(SICI)1096-9837(200004)25:4 < 397::AID-ESP62 > 3.0.CO;2-9

Scoffin, T. P. 1993. The geological effects of hurricanes on coral reefs and the interpretation of storm deposits. Coral Reefs **12**: 203–221. doi:10.1007/BF00334480

Taebi, S., R. J. Lowe, C. B. Pattiaratchi, G. N. Ivey, G. Symonds, and R. Brinkman. 2011. Nearshore circulation in a tropical fringing reef system. J. Geophys. Res. Oceans **116**: 1–15. doi:10.1029/2010JC006439

Taebi, S., R. J. Lowe, C. B. Pattiaratchi, G. N. Ivey, and G. Symonds. 2012. A numerical study of the dynamics of the wave-driven circulation within a fringing reef system. Ocean Dyn. **62**: 585–602. doi:10.1007/s10236-011-0514-4

Thieler, E. R., E. A. Himmelstoss, J. L. Zichichi, and A. Ergul. 2009. The Digital Shoreline Analysis System (DSAS) version 4.0-an ArcGIS extension for calculating shoreline change. No. 2008–1278. US Geological Survey.

Thomson, R. E., and W. J. Emery. 2014. Data analysis methods in physical oceanography. Elsevier.

Tolman, H. L. 2009. User manual and system documentation of WAVEWATCH-III^{TM} version 3.14, p. 220. Tech. note 220. NOAA/NWS/NCEP/MMAB.

Wang, P., J. H. Kirby, J. D. Haber, M. H. Horwitz, P. O. Knorr, and J. R. Krock. 2006. Morphological and sedimentological impacts of Hurricane Ivan and immediate poststorm beach recovery along the northwestern Florida barrier-island coasts. J. Coast. Res. **22**: 1382–1402. doi:10.2112/05-0440.1

Woodruff, J. D., J. L. Irish, and S. J. Camargo. 2013. Coastal flooding by tropical cyclones and sea-level rise. Nature **504**: 44–52. doi:10.1038/nature12855

Wright, L. D., and A. D. Short. 1984. Morphodynamic variability of surf zones and beaches: A synthesis. Mar. Geol. **56**: 93–118. doi:10.1016/0025-3227(84)90008-2

Yates, M. L., R. T. Guza, and W. C. O'Reilly. 2009. Equilibrium shoreline response: Observations and modeling. J. Geophys. Res. Oceans **114**: 1–16. doi:10.1029/2009JC005359

Acknowledgments

The authors thank Carlin Bowyer, Anton Kuret, Rebecca Green, Claire Ross, Michael Tropiano, George Shedrawi, Oceanwise Expeditions, and Dive Ningaloo for field assistance. This project was funded by an Australian Research Council (ARC) Future Fellowship (FT110100201), ARC Discovery Project grant (DP140102026), ARC Centre of Excellence for Coral Reef Studies (CE140100020), and by the Gorgon Barrow Island Net Conservation Benefits Fund as part of the Pilbara Marine Conservation Partnership. MC and ED were supported by UWA Scholarship for International Research Fees and University International Stipend.

Submitted 22 August 2017
Revised 29 November 2017
Accepted 30 January 2018